

Modeling of hydrogen storage materials by density-functional calculations

P. Ravindran*, P. Vajeeston, R. Vidya, H. Fjellvåg, A. Kjekshus

Department of Chemistry, University of Oslo, Box 1033, Blindern, N-0315 Oslo, Norway

Available online 24 May 2006

Abstract

Theoretical investigations on the electronic structure, chemical bonding, and ground-state and high pressure properties of metal and complex hydrides are reported. Recently a series of metal hydrides with unusually short H–H separations has been synthesized in Norway. The origin of this unexpected short H–H separation has been explained and several compounds with even shorter H–H separations have been predicted. From a systematic study on around 100 ZrNiAl-type compounds we have demonstrated that the electron localization function is a powerful tool to predict hydrogen positions in metal, intermetallic and alloy matrices. Based on these observations we have devised a new empirical rule, termed as “site-preference rule”, for prediction of suitable sites for hydrogen accommodation. First principle total-energy calculations have been carried out for AH, EH₂, AEH₃, AXH₄, and A₃XH₆ (A = alkali metal, E = alkaline earth metal, X = B, Al or Ga) compounds to study structural phase stability at ambient and high pressures. We have reproduced crystal structures of known phases and predicted structural parameters for other compounds within these series. We have found that, if the cation (A⁺ or E²⁺) radius is relatively small, one can expect several pressure-induced structural transitions with huge volume collapse at the first phase-transition point. These materials have mixed chemical bonding character which we have characterized by charge density, charge transfer, electron localization function, site- and angular-momentum projected density of states, crystal orbital Hamilton population analysis, Born effective charges, and Mulliken population analyses.

© 2006 Elsevier B.V. All rights reserved.

Keywords: Hydrogen storage materials; Chemical bonding; Electronic structure; Pressure-induced structural transition; Density functional calculations; Site occupancy

1. Introduction

Hydrogen, which has one of the highest gravimetric energy densities of any fuel, unfortunately is also the lightest of all elements. This means that typically large volumes or high pressures are required to store appreciable amount of hydrogen needed to permit a fuel cell vehicle to exhibit an acceptable operating range. Developing safe and reliable hydrogen storage technology that meet performance and cost requirements is critical to use hydrogen as a fuel for both vehicular applications and off-board uses such as for stationary power generation and for hydrogen delivery and refuelling infrastructure. In order to achieve [1] the storage capacities of 2 kWh kg⁻¹ (6 wt.% hydrogen) and 1.5 kWh L⁻¹ (0.045 kg hydrogen L⁻¹) to use hydrogen as a fuel for practical applications, the gravimetric and volumetric capacities of the hydrogen storage materials must clearly be increased than the present levels. Current

on-board hydrogen storage approaches involve compressed hydrogen gas tanks, liquid hydrogen tanks, metal hydrides, carbon-based materials/high surface area sorbants such as metal-organic frameworks, and chemical hydrogen storage using complex hydrides. Chemical storage represents one class of potential solutions to the storage problem. Metal hydrides can release hydrogen reversibly under acceptable conditions (for example LaNi₅H₆). However, these materials are too heavy and expensive for on-board vehicle applications.

For the usage of hydrogen as an ideal fuel for many types of energy converters one requires efficient and safe storage of hydrogen in the form of metal hydrides. For stationary or heavy duty vehicle applications, traditional interstitial metal hydrides have been successfully utilized [2]. Over the past few decades, a major challenge which still remains, is to identify optimal intermetallics for such purposes. Rare-earth alloys seem promising owing to high hydrogen capacity per volume unit and their ability to absorb hydrogen under moderate conditions [3,4]. The hydrogen absorption/desorption properties of these alloys are very much dependent on the constituents and the metal-hydrogen bonding interactions play a major role for the stability of the hydrides. In order to optimize hydride phases for a certain

* Corresponding author. Tel.: +47 22 855606; fax: +47 22 855441.
E-mail address: ponniah.ravindran@kjemi.uio.no (P. Ravindran).
URL: <http://folk.uio.no/ravi>.

application, an improved understanding of the role of individual alloy constituents in relation to hydrogen and the subsequent influence on electronic and structural properties are desirable.

The crystal structures of intermetallic phases are often complex and there are several potential interstices that might accommodate the hydrogen depending on factors like the size and shape of the interstitial site, chemical nature of the surrounding atoms, and the interatomic distances to hydrogen and the coordinating atoms [5,6]. Structural studies of intermetallic hydrides have revealed that empirical rules can be used to predict important features of the hydrogen sub-lattices in a given metal matrix [7,8]. The searches for efficient hydrogen-storage metal hydrides have some extent been hampered by the mental barriers which empirical rules have put on the thinking. For example, the radius of the interstitial hole which hydrogen is expected to occupy should be $>0.40 \text{ \AA}$. A survey [8] of stable hydrides shows that the minimum H–H distance does not exceed 2.1 \AA (the “2- \AA rule”). This empirical pattern is later [9] supported by band-structure calculations which ascribe the features to repulsive interaction generated by the partially charged hydrogen atoms. A practical consequence of this repulsive H–H interaction in metal hydrides is that it puts a limit to the amount of hydrogen which can be accommodated within a given structural framework. So, if H–H separations less than 2 \AA would be possible this could open for new prospects for potential candidates with higher hydrogen-storage capacity.

The structural knowledge for hydrides is by and large very limited owing to complexity in structural arrangements and difficulties involved in establishing hydrogen positions. If one know before hand the knowledge about the site preference of hydrogen in the host matrices, it will help to design new hydrogen storage materials with desired weight percentage of hydrogen. The electron-localization function (ELF) is a useful tool to characterize chemical bonding in solids. For example, Savin et al. [10] have distinguished different kinds of bonding in wide range of materials and also demonstrated that it is possible to identify the site preference for hydrogen in the Ca metal using ELF analysis. Using systematic ELF analysis of around hundred compounds in the ZrNiAl-type structural frameworks we have confirmed that ELF can reliably be used to predict the site preference of hydrogen in metals, intermetallics and alloys. Based on this observation we have developed new semi-empirical rule called “site-preference rule” for hydrogen occupation in metal matrices.

The known reversible metal hydrides which have the desired gravimetric densities, such as MgH_2 require high temperatures to release hydrogen. Currently, there is no hydrogen storage material exists which can meet all DOE 2010/FreedomCAR hydrogen storage system targets. Recently, it has been shown [11] that the complex hydride NaAlH_4 can reversibly absorb hydrogen at lower pressures and temperatures than MgH_2 and has a higher gravimetric capacity and lower cost than LaNi_5H_6 . Complex hydrides form a new class of reversible hydrides which have not been fully explored. It is possible that novel complex hydrides could have improved properties for on-board hydrogen storage. Complex hydrides of aluminium have been considered attractive as hydrogen storage compounds due to their large

hydrogen content. Unfortunately, their application in this manner has been impractical as a result of the great difficulties in reversing the hydrogen release reaction. Since workers in several laboratories reported the discovery of a number of catalysts that improve the reversing of the hydrogen release in NaAlH_4 , Na_3AlH_6 , and LiAlH_4 , interest for the use of complex hydrides of aluminium as hydrogen storage media was rekindled.

In the first part of this paper we present results on metal hydrides which have unusually short H–H separation and also analyzed the possible reasons. The predicting capability of density functional theory on site preference of hydrogen in metal matrices is also demonstrated. The second part deals with the exploration of new complex hydrides from theoretical calculations and also the structural stability of these materials at high-pressures based on total energy studies. The chemical bonding in selected complex hydrides have been analyzed with the help of partial density of states (DOS), crystal-orbital Hamilton population (COHP), charge density, charge difference and electron-localization function, Mulliken population and Born effective charges.

2. Computational details

The Vienna ab initio simulation package (VASP) [12] has been used for the total-energy calculations to establish phase stability and transition pressures. The generalized gradient approximation (GGA) [13] includes the effects of local gradients in the charge density for each point in the materials and which generally gives better equilibrium structural parameters than the local density approximation (LDA). Hence, we have used GGA for all our calculations. The ground state charge density and energy are calculated using a preconditioned conjugate gradient minimization algorithm [14] coupled with a Pulay-like mixing scheme [15]. Due to numerical instabilities associated with integrating the step-function character of the 0 K Fermi–Dirac distribution, partial occupancies of the single-particle wave functions are introduced to accelerate the convergence [16]. An energy cut-off of 400 eV was used, in the “high precision” option which guarantees that absolute energies are converged to within a few meV f.u.^{-1} . To promote cancellation of errors when calculate the total energy difference between structure, the calculations were made with same k point density for all structures within a series. The structures are fully relaxed for all volumes considered in the present calculations using force as well as stress minimization. Experimentally established structural data were used as input for the calculations when available, or closely related structures were considered to identify ambient and high-pressure phases. The PAW pseudo-potentials [17] were used for all our calculations. A criterion of at least $0.01 \text{ meV atom}^{-1}$ was placed on the self-consistent convergence of the total energy. The present type of theoretical approach has recently been successfully applied [18–21] to reproduce ambient- and high-pressure phases computationally.

The modern theory of macroscopic polarization [22] allows the calculation of Born effective charge Z^* using Berry phase approach implemented in the VASP code. To have more insight into the bonding behavior of complex hydrides, we have

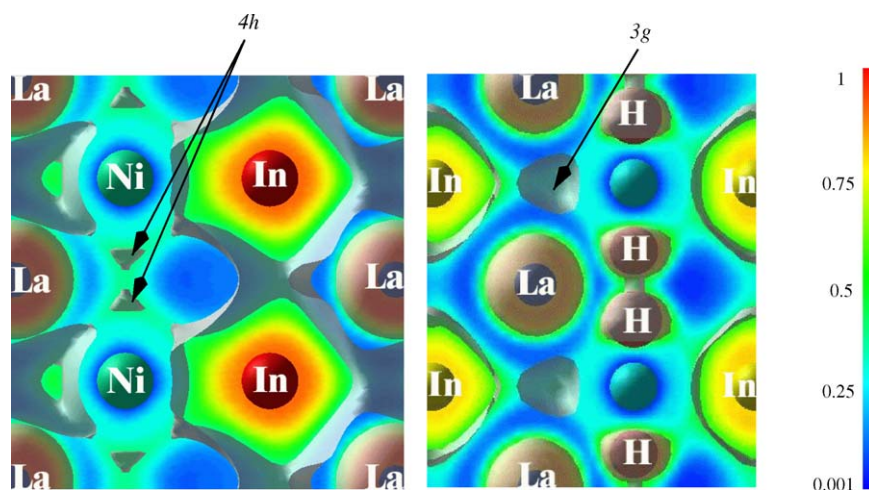


Fig. 1. Calculated ELF in the (001) plane for LaNiIn and LaNiInH_{1.333}. Different crystallographic site (4h and 3g) are marked by arrows. The *iso*-surface values correspond to 0.6 ELF value. Legends for different kinds of atoms are given on the illustration.

calculated Born effective charges using finite differences. The chemical bonding in complex hydrides are also analyzed with the help of Mulliken population analyses as implemented in CRYSTAL03 package [23]. For the structural optimization for metal hydrides we have used the full-potential linear muffin-tin-orbital method [24].

3. Results and discussion

3.1. Site preference of hydrogen in metal matrices

In order to design new metal hydrides for hydrogen storage applications a main prerequisite is the knowledge about the site preference of hydrogen in the corresponding non-hydride phases. The shortest H–H separation between two hydrogen atoms in a crystalline framework is limited by the H-to-H repulsion and it is commonly believed that two hydrogen atoms cannot be located closer together than some 2.0 Å [8]. This so-called “2-Å rule” appears to hold for the absolute majority of precisely described structures of metal (alloy/intermetallic) hydrides. In contrast, a recent experimental study [25] on RNiIn (R = La, Ce, Nd; generally a rare-earth element) series shows that hydrides of these compounds violate the “2-Å rule” vigorously. Using density functional calculations we have explained [26,27] the origin for the violation and suggested that the H–H separation may be reduced to even below 1.5 Å, by combinations of other element. ELF is a measure for the probability distribution of paired electrons, and this function is able to better distinguish different bonding situations for electrons than the plain charge-density distribution [28]. Savin et al. [10] demonstrated that it is possible to identify the site preference for hydrogen in the Ca metal using ELF analysis.

Using the help of ELF, if one able to predict correctly the site preference of hydrogen in RNiIn compounds, then this approach can reliably be used to predict site preference of hydrogen in metal matrices. According to experimental neutron diffraction measurements, hydrogen occupies the 4h sites of space group *P62m* with full occupancy [25]. Interestingly our ELF diagram

for LaNiIn shown in left panel of Fig. 1 has higher value of ELF at the 4h sites than other interstitial sites. The higher value of ELF at the 4h site indicates that electrons at that site are having nonbonding localized nature than other possible interstitial sites. It appears that hydrogen prefers to occupy the interstitial sites those have relatively more nonbonding localized electrons in metal matrices. So, consistent with experimental observations [25], ELF analysis correctly predicts the site preference of hydrogen in LaNiIn.

On this background it is interesting to visualize the ELF for LaNiInH_{1.333} (see right panel in Fig. 1) to look for possible interstitial sites where hydrogen prefers to occupy. With the 4h site filled up by hydrogen, another interstitial site (3g) with an ELF value of around 0.6 appears (while other interstitial sites still show negligible ELF levels). A recent study about deuteration of LaNiIn under pressure ($pD_2 = 4.6$ bar) has revealed a new phase, LaNiInD_{1.64}, in which deuterium occupies both the 4h (96% filled) and 3g (36% filled) sites. The structural optimization for the corresponding filled-up LaNiInH_{2.333} structure gave unit-cell dimensions and positional parameters in satisfactory agreement (*viz.* within the expected accuracy for DFT calculations) with the experimental findings for LaNiInD_{1.64}. We have also calculated the hydride formation energies for all these compounds and the conclusions arrived from ELF analysis is consistent with the results obtained from our hydride formation energy calculations [29].

It was indeed the success of ELF to correctly predict the site preference of hydrogen in just discussed hydride phases led us to undertake a more systematic study of the ZrNiAl-type family. Based on this systematic study we proposed [29] a “site-preference rule” for hydrogen in metal matrices which says that hydrogen prefers to occupy the interstitial sites where electrons have relatively more nonbonding localized nature than other possible sites in metals, metal matrices and intermetallic frameworks. The origin of the site-preference rule is that, when hydrogen atom is diffused into the metal matrices it tries to find a place in the metal matrix where it can find electrons that can easily participate in the bonding interaction such that it can achieve

a more stable $1s^2$ paired electron configuration and thereby completes its valence shell.

The insertion of hydrogen in the metal matrix causes highly anisotropic lattice changes; a large expansion along c and a small contraction in the a direction. Among the studied hydrides, the hypothetical $\text{LaPtInH}_{1.333}$ phase exhibits the shortest H–H separation (1.454 Å). The optimized unit-cell parameters and atomic coordinates fit very well with the experimental findings for $\text{RNiInH}_{1.333}$, $R = \text{La, Ce, and Nd}$ [27]. From the systematic studies on series of metal hydrides we have found that hydrogen always accept charges from the metallic host lattice and present in the negatively charged condition at the metal hydrides. The negatively charged particle will have repulsive Coulomb interaction and hence the hydrogen atoms in metal hydrides are well separated from each other (the H–H separation is generally higher than 2 Å) compared to that in hydrogen molecule (the H–H separation is 0.746 Å). In $\text{RNiInH}_{1.333}$ compounds the electrons at the H sites are polarized toward the electropositive In atoms and also the H–H repulsive interaction has been screened by the rare-earth ions present in the systems [26]. These are the reasons for the unusually short H–H separation in $\text{RNiInH}_{1.333}$.

3.2. Chemical bonding in complex hydrides

3.2.1. Crystal-orbital Hamilton-population analysis

To gauge the bond strength we have used crystal-orbital Hamilton-population, COHP, analyses, as is implemented in the TBLMTO-47 package [35]. The COHP (viz. the Hamiltonian-population-weighted DOS) is identical with the crystal-orbital-overlap population. Ideally the COHP takes a negative value for bonding and positive for antibonding states. In order to illustrate the bond strength between the constituents, the COHP between atoms in KAlH_4 is shown in Fig. 2 taking all valence orbitals into account. From this illustration it seems clear that the strongest bond in KAlH_4 is between Al and H. There is considerable covalent interaction between Al and H. Both bonding and antibonding states are present in the COHP between the H atoms at the VB, and hence the bonding interaction between the H atoms may be considered as weak. Owing to the ionic bonding between K and H, the COHP between these atoms is small. The integrated COHP values give the bonding interactions between atoms quantitatively and those between Al–H, K–H, H–H, and K–Al are -0.978 , -0.042 , -0.015 , and -0.017 eV, respectively.

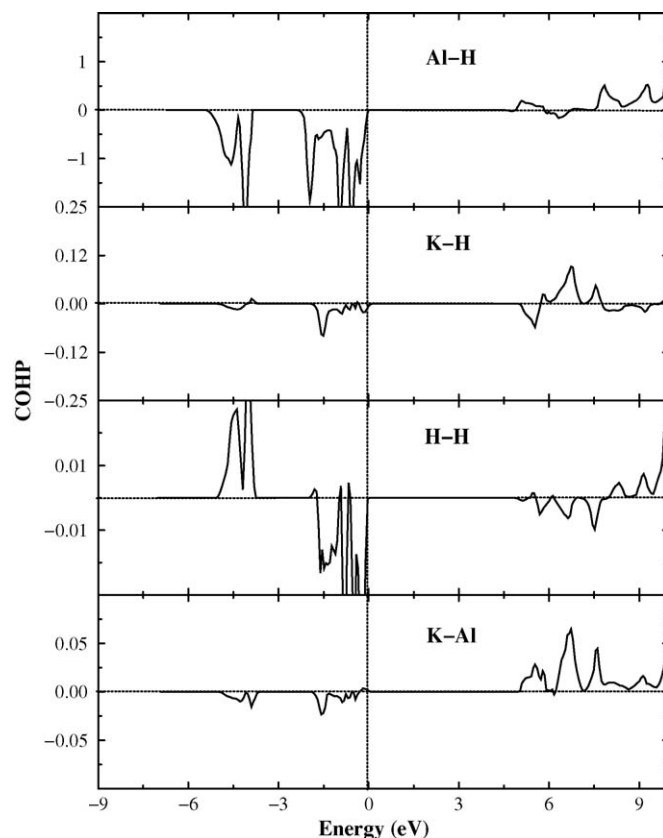


Fig. 2. COHP between different constituents for KAlH_4 . Fermi level is set to zero and marked by the vertical line.

One of the disadvantages of using complex hydrides for practical application is the requirement of high temperatures to take out hydrogen from these materials. From our COHP analysis it is clear that if one could able to weaken the bonding interaction between Al and hydrogen, one can reduce the temperature to take out hydrogen.

3.2.2. Charge density, charge difference, and ELF

In order to improve the understanding about the bonding interactions, the calculated valence-charge-density distribution for KAlH_4 is depicted in Fig. 3a. From this illustration it appears that Al and H form an AlH_4 molecule-like structural subunits and the bonding interaction between Al and H is of covalent character. Moreover, Fig. 3a demonstrates that there is

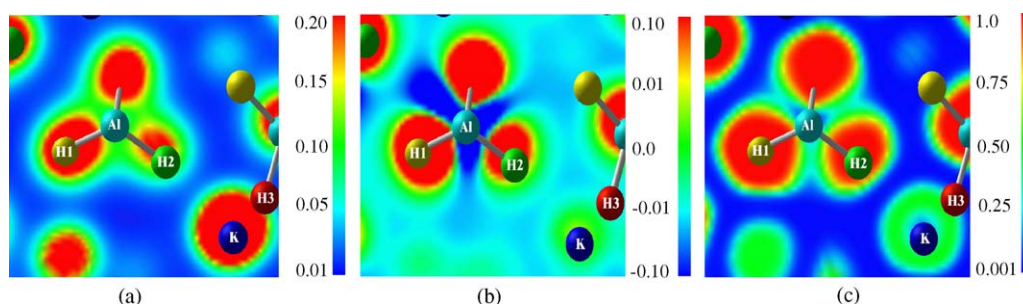


Fig. 3. (a) Total charge density, (b) charge transfer, and (c) electron localization function plot for KAlH_4 .

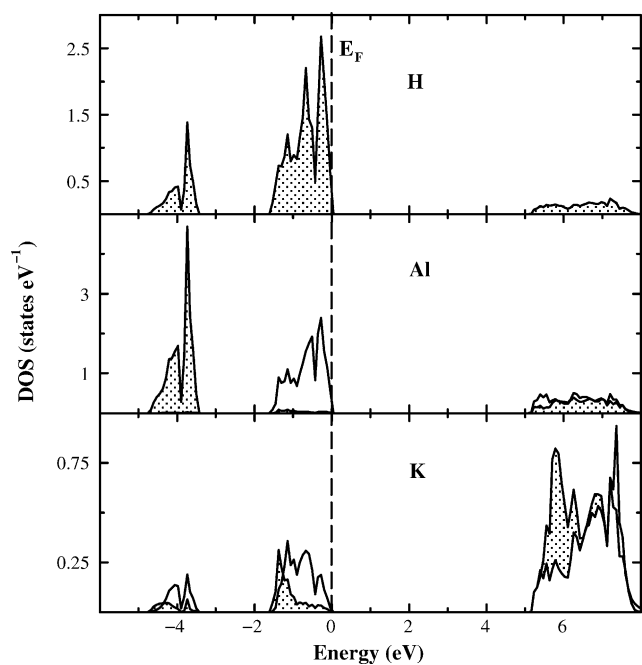


Fig. 4. The calculated angular-momentum-projected density of states for KAlH_4 . The s-states are shown with shade and the Fermi level is set to zero and marked by the vertical line.

no substantial charge density distributed between K atoms and the AlH_4 structural subunits. This clearly indicates the presence of ionic bonding. In order to depict the role of charge transfer we have displayed the charge transfer plot (the difference in the electron density of the compound and that of constituent atoms superimposed on the lattice grid) for KAlH_4 in Fig. 3b. From Fig. 3b it is clear that electrons are transferred from K and Al to the H sites. But the charge transfer from Al is not isotropic as clearly seen from Fig. 3a. The anisotropic charge transfer from Al to the H sites indicates the presence of ionic-covalent bonding between Al and H.

The ELF is an informative tool to distinguish different kinds of bonding interactions in solids [10], and the ELF for KAlH_4 is given in Fig. 3c. The large value of ELF at the H site indicates strongly paired electrons with local bosonic character. The negligibly small ELF between K and H, and the small value of ELF at the K site with spherically symmetric distribution indicate that the bonding interaction between K and H is purely ionic. The ELF distribution at the H site is not spherically symmetric and it is polarized towards Al atoms indicate the presence of directional bonding between Al and H.

3.2.3. Density of states analysis

The calculated partial density of states for KAlH_4 given in Fig. 4 clearly shows that this material is a wide band gap insulator with the band gap of 5.2 eV. Generally the band gap value of all the AAIH_4 materials is of the order of 5 eV [19,20]. When one replaces the Al atoms by boron atoms, the band gap increases owing to the increase of covalent bonding interaction between hydrogen and boron. Hence, the band gap value varies between 5.5 eV for CsBH_4 to 7.0 eV for LiBH_4 [36]. If one replaces the Al atom with Ga, we found that the band gap value decreases

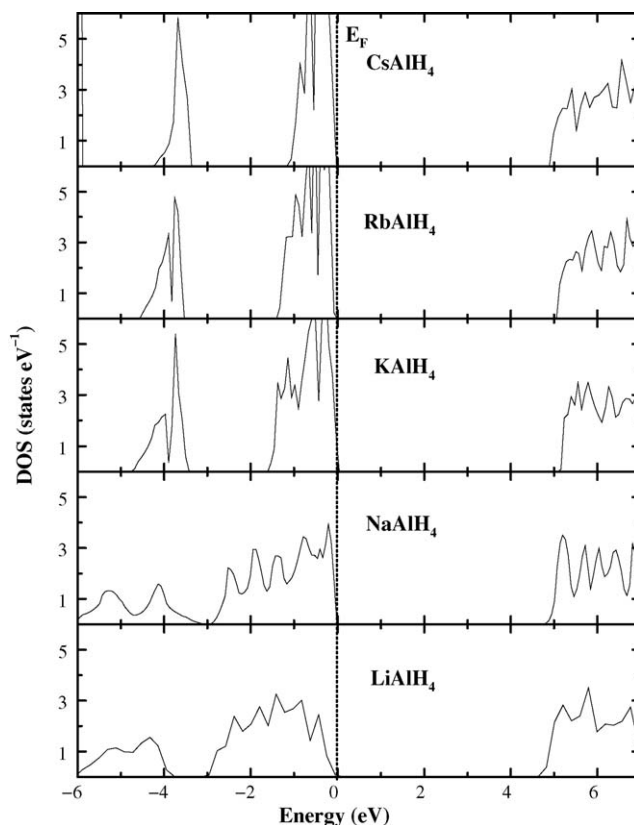


Fig. 5. The calculated total density of states for AAIH_4 . The Fermi level is set to zero and marked by the vertical line.

[37]. The calculated band gap (E_g) for these compounds varies from 4.57 for LiGaH_4 to ≈ 5 eV for CsGaH_4 compound.

The valence band of these compounds consists of two well separated regions. In the case of KAlH_4 , the lower energy region of VB around -4 eV contains mainly Al-s and H-s electrons with small contribution coming from K atoms. These states are the bonding states originating from hybridization interaction between Al and H. The top of the VB is dominated by H-s states as well as Al-p states which are energetically degenerate implying the presence of covalent bonding between Al and H. Considerably small value of DOS at the K site indicates the ionic bonding between K and AlH_4 .

The total DOS (Fig. 5) for the AAIH_4 phases comprises three well separated regions; region I: below -5 eV, region II: from -3 to 0 eV, and region III: above 5 eV (unoccupied states; see Fig. 5). On going from LiAlH_4 to CsAlH_4 the width of the bands (in particular the VB; see Fig. 5) is narrowed. Recalling that the Al–H distance does not vary much along the AAIH_4 series it seems safe to conclude that it is the enhancement in the A–H interaction which is the main reason for the reduction in the VB width. Also, on going from Li to Cs systems the energy separation between the two peaks at the VB systematically increases. This indicates that the ionicity of the system increases. The DOS at the VB region for LiAlH_4 and NaAlH_4 are having broad features than other three compounds in Fig. 5 indicating that the hybridization interaction between atoms in these two systems is relatively larger (Table 1).

Table 1
Calculated a , c (in Å), and c/a for LaTiIn and LaTiInH_{1.333}; and changes $\Delta a/a$, $\Delta c/c$, and $\Delta V/V$ (%) on hydrogenation

Compound	a		c		c/a		$\Delta a/a$		$\Delta c/c$		$\Delta V/V$	
	Theoretical	Experimental	Theoretical	Experimental	Theoretical	Experimental	Theoretical	Experimental	Theoretical	Experimental	Theoretical	Experimental
LaNiIn	7.5604	7.5906 ^a	3.9924	4.0500 ^a	0.5281	0.5336 ^a	–	–	–	–	–	–
LaNiInH _{1.333}	7.3771	7.3810 ^a	4.6254	4.6489 ^a	0.6270	0.6399 ^a	–2.43	–2.76	15.86	14.80	10.31	8.54
LaPdIn	7.7716	7.7290 ^b	4.1250	4.1330 ^b	0.5307	0.5347 ^b	–	–	–	–	–	–
LaPdInH _{1.333}	7.3501	–	4.8112	–	0.6546	–	–5.42	–	16.64	–	4.33	–
LaPtIn	7.7277	7.6950 ^b	4.1144	4.1250 ^b	0.5324	0.5361 ^b	–	–	–	–	–	–
LaPtInH _{1.333}	7.7274	–	4.6903	–	0.6070	–	–0.04	–	13.98	–	14.00	–

^a Ref. [26].

^b Ref. [30].

Table 2

Mulliken population analysis for selected hydrogen-containing compounds

Compound	Atom	MEC	Overlap population
LiH	Li	+0.98	–0.003 (Li–H)
	H	–0.98	
MgH ₂	Mg	+1.87	–0.040 (Mg–H)
	H	–0.93	
BeH ₂	Be	+1.63	0.045 (Be–H)
	H	–0.82	
AlH ₃	Al	+2.22	0.091 (Al–H)
	H	–0.74	
LiAlH ₄	Li	+1.01	0.171 (Al–H)
	Al	+2.01	
	H	–0.75	
Li ₃ AlH ₆	Li	+1.01	0.105 (Al–H)
	Al	+2.08	
	H	–0.85	

The Mulliken effective charges (MEC) are given in terms of e .

3.2.4. Mulliken population analysis and Born effective charges

In order to make a quantitative conclusion about bonding interactions between constituents it would be useful to identify the amount of electrons on a particular atom and populations between atoms. Although there is no unique definition of how many electrons are associated with an atom in a molecule or a sub-unit of a solid, it has nevertheless proved useful in many cases to perform population analyses. Due to its simplicity the Mulliken [38] population scheme has become the most familiar approach to count electrons associated with a given atom. However, this method is more qualitative than quantitative, giving results that are sensitive to the atomic basis. Mulliken charges are reported in Table 2 for some saline-like (LiH, BeH₂ and MgH₂) and complex hydrides. LiH is considered as a pure ionic compound and the calculated Mulliken charges reflect nearly pure ionic picture with Li⁺ and H[–]. The overlap population between Li⁺ and H[–] is also close to zero, as expected for an ionic compound. Similarly, the case of MgH₂, BeH₂, and AlH₃ the bonding interaction is mainly ionic, but the degree of ionicity is reduced from MgH₂ to BeH₂ and further to AlH₃, viz. these compounds exhibit some covalent character as evidenced by the non-zero overlap population. The Mulliken effective charges for Li, Al, and H in LiAlH₄ and Li₃AlH₆ indicate that the interaction between the Li and AlH₄/AlH₆ is ionic. There is a finite overlap population between Al and H within the AlH₄/AlH₆ units which reflects the presence of partial covalent character of the Al–H bond. However, the magnitude of overlap population is smaller than that for pure covalent compounds. Also, the partial charges (around two electrons transferred from Al to H) imply the presence of significant ionic contribution in the Al–H bond.

Born effective charge is another quantity to analyze the bonding character of the materials. We used the King-Smith and Vanderbilt [39] method to calculate the polarizations of perturbed cells and from this the Born effective charge tensors of the ions have been calculated. In Table 3 the calculated Born effective

Table 3
Calculated Born effective charge tensors for Li_3AlH_6

	xx	yy	zz	xy	yz	zx	xz	zy	yx
Z_{Li}^*	0.990	0.957	0.985	0.017	0.102	0.014	0.061	0.024	0.102
Z_{Al1}^*	2.237	2.237	1.735	0.034	−0.001	0.000	−0.001	0.000	−0.001
Z_{Al2}^*	2.024	2.024	2.251	0.024	−0.001	0.000	0.000	0.000	−0.001
Z_{H1}^*	−1.018	−0.738	−0.846	0.082	0.027	−0.174	−0.190	0.073	0.027
Z_{H2}^*	−0.911	−0.831	−0.817	−0.088	0.125	0.210	0.153	0.116	0.125

tive charge tensors for the constituents in Li_3AlH_6 are tabulated. For Li and Al, the diagonal components of effective charges in the Cartesian frame are $Z_{xx} = Z_{yy} \neq Z_{zz}$ and the off-diagonal components are negligible. However, at the H site, finite value of effective charges are present in the diagonal as well as off-diagonal components along with their anisotropic distribution implies that a finite directional bonding is present in this material. If the interaction is purely ionic, then one can expect that the effective charges along the diagonal component should be equal and the off-diagonal may vanish. It can be seen from Table 3 that the dynamical charge for Li is close to the nominal ionic charge (+1 for Li). For Al, its dynamical charges are 1.735–2.24, which are smaller than the nominal charge of +3. This indicates that part of the Al charges also participate in the directional bonding.

3.3. Prediction of new complex hydrides

Considerable research is being conducted to develop hydride compounds that can store hydrogen with high volumetric and gravimetric densities, and charge/discharge it reversibly under the temperature of 80–100 °C and 1 bar absolute pressure operation conditions. The current renaissance in hydrogen storage research was sparked by the discovery of catalyzed NaAlH_4 compositions that have theoretically 5.6 wt.% accessible hydrogen and are reversible under moderate temperature and pressure conditions [12]. Recent experimental evidence shows that reversible hydrogen absorption/desorption proceeds smoothly in KAlH_4 without introduction of a catalyst [40]. From this observation it appears that it may be possible to have complex hydrides with good kinetics those are yet to be identified. In this background we are exploring new complex hydrides using density functional calculations. So far we have searched new compounds in AXH_4 ($A = \text{Li, Na, K, Rb or Cs}$; $X = \text{B, Al, or Ga}$), A_3XH_6 , and EXH_5 ($E = \text{Be, Mg, Ca, Sr or Ba}$) series. From this theoretical exploration we have identified several new hydrogen storage materials and their ground state as well as high-pressure structural properties are predicted.

The uncertainty associated with the determination of coordinates of hydrogen by X-ray diffraction is large, and the thus derived metal–hydrogen distances tend to come out too short or deviate considerably from the reality. In general, compared with systems such as oxides, structural understanding of hydrides is very defective and fragmentary [41]. It is now well documented that first principle calculations can reliably be used to predict structural parameters of hydrogen storage materials

[19–22,27,36,37,42–44]. From the systematic studies on structural phase stability of around 50 compounds we found that these compounds generally have tetrahedra (XH_4) or octahedra (XH_6) structural subunits. Depending upon the radius of the cations these polyhedra get tilted and/or rotated which make different crystal structures for these compounds. The calculated total energy versus volume curves for RbAlH_4 and CsAlH_4 are given in Fig. 6a and b, respectively. The structural parameters for these two compounds are not available for comparison. Interestingly both these compounds stabilize in the orthorhombic structure. The structural parameters for all the AAIH_4 compounds obtained from our theoretical explorations are given in Table 4. For LiAlH_4 , NaAlH_4 , and KAlH_4 the structural parameters are available experimentally. From the table it should be noted that the deviation in the predicted structural parameters from experimental values for these compounds are within 3%. In the case of KAlH_4 we have first predicted [43] the structural parameters and followed by our report, neutron diffraction study [34] has been made on this compound. The structural parameters for RbAlH_4 and CsAlH_4 are given in Table 4 and no experimental results are available for these compounds. We hope that the present results will motivate experimental studies on these systems.

Both RbAlH_4 and CsAlH_4 crystallize in the orthorhombic KGaH_4 -type structure with space group $Pnma$. This structure consists of slightly distorted $[\text{AlH}_4]^-$ tetrahedra which are separated by intermittent Rb/Cs cations. In KAlH_4 , the interatomic Al–H distance within the $[\text{AlH}_4]^-$ tetrahedra varies only by 0.9% and the bond length is as expected for an anionic complex of Al and H [45]. Each K^+ cation is surrounded by 12 H atoms at distances varying between 2.717 and 3.204 Å. In the case of RbAlH_4 , we found that the energy difference between the ground state structure and α - LiAlH_4 -type structure (Fig. 6) is very small. We have identified a high-pressure modification around 7 GPa in α - RbAlH_4 and it transforms in to β - RbAlH_4 (β - NaAlH_4 -type structure) and the volume collapse at the phase transition point is relatively larger value of 12.6% (see Table 4 and also Fig. 7).

It is interesting to note that: at 2.6 GPa α - LiAlH_4 (prototype structure) transforms to β - LiAlH_4 (α - NaAlH_4 -type) and a subsequent transition from β - to γ - LiAlH_4 (KGaH_4 -type) is established at 33.8 GPa. The important aspect of the α -to- β transition in LiAlH_4 is the small energy difference [19] between the involved phases (only 11.56 meV f.u.^{−1}), or 1.154 kJ mol^{−1}, which is indeed much smaller than that found for other hydrides [21] and oxides [46]. At the α -to- β transition point for LiAlH_4

Table 4
 Calculated cell parameters (Å), unit-cell volume (Å³), positional parameters, bulk modulus (B_0 in GPa) and pressure derivative (B'_0), and volume discontinuities (%) at phase transition points for MAIH₄ compounds

Compounds (structure type; space group)	Unit-cell dimension	Unit-cell volume	Positional parameters	B_0	B'_0	ΔV
α -LiAlH ₄ (proto type; $P2_1/c$)	$a = 4.8535$ (4.8174) ^a	65.24	Li: 0.5699, 0.4652, 0.8245 (0.5603, 0.4656, 0.8266) ^a Al: 0.1381, 0.2017, 0.9319 (0.1386, 0.2033, 0.9302) ^a H1: 0.1807, 0.0986, 0.7630 (0.1826, 0.0958, 0.7630) ^a H2: 0.3542, 0.3723, 0.9777 (0.3524, 0.3713, 0.9749) ^a H3: 0.2361, 0.0810, 0.1146 (0.2425, 0.0806, 0.1148) ^a H4: 0.7948, 0.2633, 0.8717 (0.7994, 0.2649, 0.8724) ^a	12.95	4.10	–
	$b = 7.8259$ (7.8020) ^a					
	$c = 7.8419$ (7.8214) ^a					
	$\beta = 111.878^\circ$ (112.228 ^o) ^a					
β -LiAlH ₄ (α -NaAlH ₄ -type; $I4_1/a$)	$a = 4.6611^b$ (4.7312) ^c	59.96	Li: (0, 1/4, 5/8) ^{b,c} ; Al: (0, 1/4, 1/8) ^{b,c} H: (0.2527, 0.4237, 0.5413) ^b (0.2492, 0.4191, 0.5429) ^c	25.64	4.35	17
	$c = 10.5219^b$ (10.7161) ^c					
γ -LiAlH ₄ (KGaH ₄ -type; $Pnma$)	$a = 5.4421$	134.77	Li: (0.2428, 1/4, 0.2467) ^b (0.2497, 1/4, 0.2502) ^c Al: (0.5120, 1/4, 0.8221) ^b (0.5002, 1/4, 0.7361) ^c H1: (0.3067, 1/4, 0.9617) ^b (0.2815, 1/4, 0.9617) ^c H2: (0.7162, 1/4, 0.9631) ^b (0.7189, 1/4, 0.9467) ^c H3: (0.4889, 0.9833, 0.2943) ^b (0.4998, 0.9173, 0.3279) ^c	14.25	4.85	4
	$b = 4.4843$					
	$c = 5.5225$					
α -NaAlH ₄ (proto type; $I4_1/a$)	$a = 4.9965$ (4.9801) ^d	69.15	Na(4a): 0, 1/4, 1/8 Al(4b): 0, 1/4, 5/8 H(16f): 0.2199, 0.3710, 0.5639 (0.2372, 0.3869, 0.5456) ^d	19.29	3.9	–
	$c = 11.0828$ (11.1483) ^d					
β -NaAlH ₄ (SrMgH ₄ -type; $Cmc2_2$)	$a = 3.5493$	62.75	Na(4a): 0, 0.1695, 0.2409 Al(4a): 0, 0.4139, 0.2047; H1(4a): 0, 0.3476, 0.4877 H2(4a): 0, 0.3105, 0.0116; H3(4a): 0, 0.0751, 0.6811 H4(4a): 0, 0.5269, 0.3739	38.41	3.1	4
	$b = 13.8304$					
	$c = 5.1133$					
KAlH ₄ (KGaH ₄ -type; $Pnma$)	$a = 8.8249$ (8.814) ^e	95.49	K(4c): (0.1778, 1/4, 0.1621) ^b (0.1775, 1/4, 0.1598) ^f Al(4c): (0.5663, 1/4, 0.8184) ^b (0.5659, 1/4, 0.8201) ^f H1(4c): (0.4034, 1/4, 0.9184) ^b (0.4063, 1/4, 0.9611) ^f H2(4c): (0.7055, 1/4, 0.9623) ^b (0.7153, 1/4, 0.9611) ^f H3(8d): (0.4194, 0.9810, 0.3127) ^b (0.4181, 0.9701, 0.3137) ^f	10.34	4.61	–
	$b = 5.8590$ (5.819) ^e					
	$c = 7.3872$ (7.331) ^e					
α -RbAlH ₄ (KGaH ₄ -type; $Pnma$)	$a = 9.4708$	107.39	Rb(4c): 0.1816, 1/4, 0.1597 Al(4c): 0.0615, 1/4, 0.6863 H1(4c): 0.0983, 3/4, 0.3989 H2(4c): 0.3117, 3/4, 0.0389 H3(8d): 0.0802, 0.0238, 0.8121	9.2	5.2	–
	$b = 5.9075$					
	$c = 7.6779$					
β -RbAlH ₄ (SrMgH ₄ -type; $Cmc2_2$)	$a = 3.9933$	94.35	Rb(4a): 1/2, 0.6206, 0.2833 Al(4a): 1/2, 0.1154, 0.7607	14.1	3.5	12.6
	$b = 14.6472$					

Table 4 (Continued)

Compounds (structure type; space group)	Unit-cell dimension	Unit-cell volume	Positional parameters	B_0	B'_0	ΔV
α -CsAlH ₄ (KGaH ₄ -type; <i>Pnma</i>)	$c = 6.4933$	123.4	H1(4a): 1/2, 0.7996, 0.0670 H2(4a): 1/2, 0.1717, 0.9990 H3(4a): 1/2, 0.5992, 0.7814 H4(4a): 1/2, 0.9888, 0.1074	8.6	4.6	3.8
	$a = 9.9249$		Cs(4c): 0.1847, 1/4, 0.1629			
	$b = 6.1988$ $c = 8.0198$		Al(4c): 0.0594, 1/4, 0.6970 H1(4c): 0.1087, 3/4, 0.3821 H2(4c): 0.3125, 3/4, 0.0418 H3(8d): 0.0812, 0.0180, 0.8256			
β -CsAlH ₄ (α -NaAlH ₄ -type)	$a = 4.3887$	108.1	Cs(4a): 0, 3/4, 1/8	9.5	5.1	
	$b = 11.2137$		Al(4b): 1/2, 3/4, 7/8; H(16h): 0.7622, 3/4, 0.9434			
γ -CsAlH ₄ (SrMgH ₄ type; <i>Cmc2₂</i>)	$a = 3.6619$	85.3	Cs(4a): 1/2, 0.6159, 0.2871	9.1	4.9	9.3
	$b = 14.2468$ $c = 6.51766$		Al(4a): 1/2, 0.1221, 0.7546 H1(4a): 1/2, 0.79419, 0.08073 H2(4a): 1/2, 0.1649, 0.9874 H3(4a): 1/2, 0.6072, 0.7706 H4(4a): 1/2, 0.9789, 0.1186			

^a Experimental values from Ref. [31].

^b Calculated values at equilibrium.

^c Calculated values at transition point.

^d Experimental values from Ref. [32].

^e From XRD measurements [33].

^f From neutron diffraction [34].

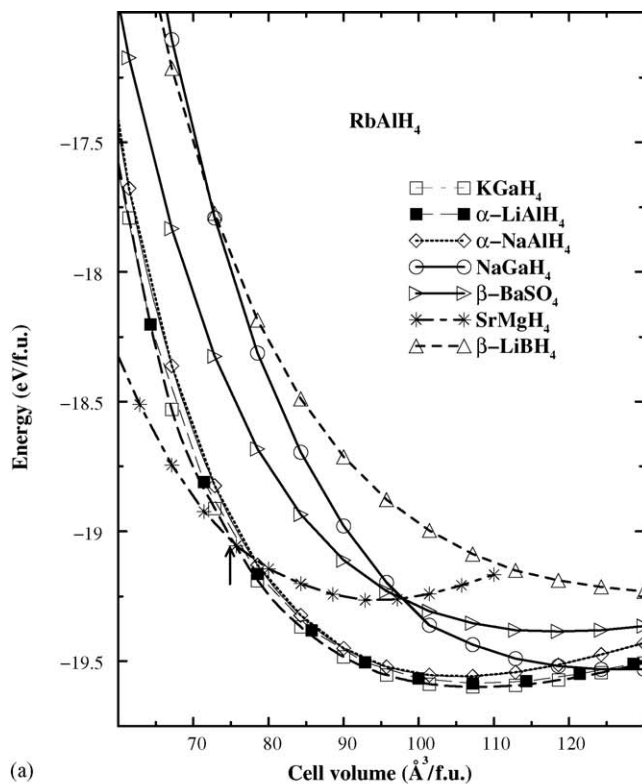
the estimated difference in cell volume is ca. 17% (Fig. 7) [19]. The Raman scattering measurement on the high-pressure phase also indicates the presence of a large volume collapse at the transition point [47]. Comparison on the basis of the equilibrium volumes for α - and β -LiAlH₄ show an even larger volume difference (viz. a huge value of 22%), which to our knowledge is the first establishment of such huge volume change at a transition point in hydrides. For example, in NaAlH₄ the calculated volume difference at the transition point between α and β phases is less than 4% [20]. It should be noted that β - and γ -LiAlH₄ have almost the same volume at the β -to- γ transition point. The relatively small equilibrium volume of β -LiAlH₄ along with its high weight content of hydrogen implies an increased hydrogen storage capacity and therefore it would be of interest to explore the possibility of stabilizing this phase by chemical means. Moreover, this phase may have improved kinetics, because the bonding behavior of the β phase is drastically different from that of the α phase.

We have calculated the total energy as a function of unit-cell volume for 12 different volumes and fitted the results to the so-called universal equation state [48] and thus obtained bulk moduli (B_0) and its pressure derivatives (B'_0) for all the AAlH₄ compounds at ambient and high pressures (see Table 4). All these compounds exhibit very small bulk modulus at the ground state structure compared with metal hydrides implying that AAlH₄ are very soft and easily compressible materials. The co-ordination number (CN) of Al changes from 4 in α -

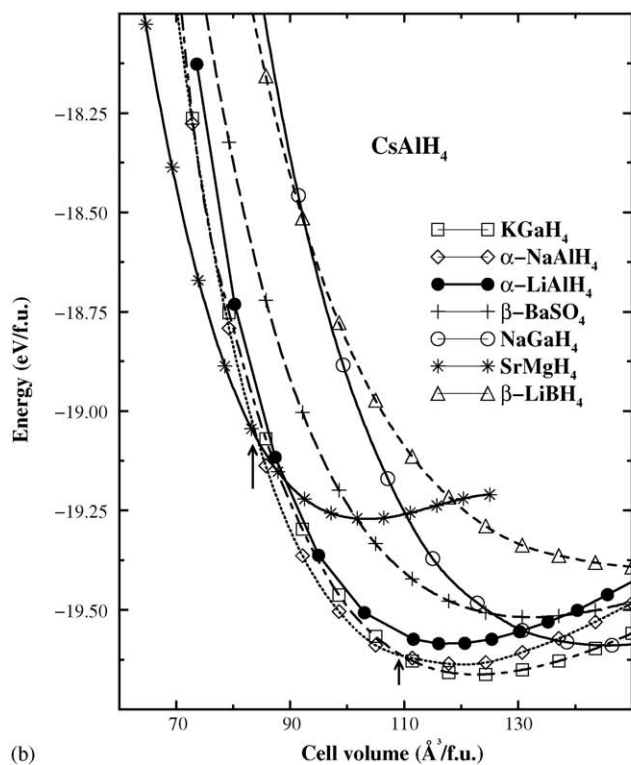
RbAlH₄ to 6 in the β -phase, viz. consistent with the expected general trend of increasing CN with weakening of the covalent bonding by increasing pressure. B_0 for β -RbAlH₄ is almost twice that of the α -phase and this is associated with large volume collapse at the phase transition point. Also, the slope of the pressure–volume curve (see Fig. 7) for β -RbAlH₄ is larger than that of α -RbAlH₄ indicating that the high-pressure phase is intrinsically harder than the ground state phase and this is largely due to the increased CN and the lower equilibrium volume of β -RbAlH₄.

Like α -RbAlH₄, α -CsAlH₄ also stabilizes in the orthorhombic structure with space group *Pnma*. The bulk modulus for α -CsAlH₄ is smaller than all the other AAlH₄ compounds which is associated with the large equilibrium volume. Moreover, the ionic radius for Cs is larger than other alkali metals and also the valence electrons of Cs are more delocalized than other alkali metals. These make α -CsAlH₄ the softest among all the AAlH₄ compounds. Similar to LiAlH₄, the total energy studies (see Fig. 6b) on CsAlH₄ also show two structural phase transitions one at 4 GPa from orthorhombic α -CsAlH₄ to tetragonal β -CsAlH₄, and around 8 GPa from tetragonal β -CsAlH₄ to orthorhombic γ -CsAlH₄ with the volume collapse of 3.8 and 9.3%, respectively. Unlike other AAlH₄ compounds the bulk modulus for CsAlH₄ in all the three phases are almost the same.

Similar to alkali aluminohydrides, alkaline-earth hydrides with low cation radii also exhibit a huge volume collapse at



(a)



(b)

Fig. 6. Total energy vs. volume curves for (a) RbAlH_4 and (b) CsAlH_4 for different possible structural arrangements. The arrows indicate the total energy cross-over point where the structural transitions take place.

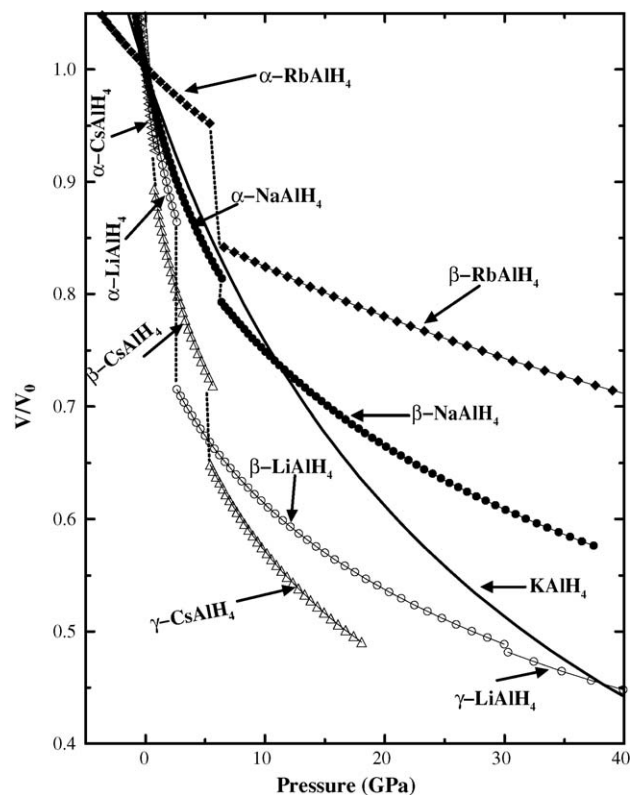


Fig. 7. Equation of states data for alkali aluminohydrides.

the first pressure-induced phase transition point. Application of pressure transforms α - to β - BeH_2 at 7.07 GPa with a calculated volume discontinuity at the transition point of ca. 19.2% (ca. 26.4% equilibrium volume difference) and a energy difference of ~ 0.4 eV [22]. Such a huge pressure-induced volume collapse is rather uncommon among hydrides as well as inorganic compounds in general. However, large volume collapses (9–20%) under pressure are observed for lanthanides and actinides associated with the valence transition or localized-to-delocalized transition of f electrons in these systems. Like in alkali aluminohydrides, we observed several pressure-induced structural transitions for alkaline-earth hydrides with small cation. For BeH_2 and MgH_2 we have found four pressure-induced structural transitions whereas only one pressure-induced structural transition was observed for BaH_2 [49]. From these systematic studies it appears that if the ionic radius of the cation is small, one can expect several pressure-induced structural transitions in main group metal hydrides and particularly huge volume collapse at the first phase transition. Interestingly, in alkali aluminohydrides we observed several pressure-induced structural transitions when they also have smaller cation radius.

4. Conclusions

From the systematic studies on metal hydrides we have shown that one can pack hydrogen atoms more efficiently in metal hydrides than the general belief. The electron localization function is a useful tool to predict site preference

of hydrogen in metal hydrides. Based on this observation we generalized an empirical site-preference rule which states that “Hydrogen prefers to occupy the interstitial sites where electrons have relatively more nonbonding localized nature than other possible sites in metals, alloys and intermetallic frameworks”.

Industries are looking for hydrogen storage materials with high wt.% of hydrogen and good hydrogen absorption/desorption kinetics. The existing phases lack one or both of them. One strategy is to explore new compounds using accurate density functional total energy calculations and solve the crystal structures of thus identified stable compounds theoretically and try to synthesize them to check for good kinetics. We have made structural optimization studies on a series of complex hydrides and the crystal structures of several new compounds have been predicted. As the known stable complex hydrides lack sorption kinetics, it is important to identify possible metastable phases in potential hydrides and try to stabilize them by suitable thermo/chemical processing conditions. From our high-pressure studies we identified several high pressure phases in these materials and in particular we found large volume collapse at the first phase transition point in several potential hydrogen storage materials. Also, the chemical bonding behavior of these high-pressure phases are drastically different from that of ambient pressure phase and hence it is expected that the metastable phases may improve the hydrogen absorption/desorption kinetics.

Detailed analysis has been made about the chemical bonding behaviors of complex hydrides using charge density, charge transfer, electron localization function, partial densities of states, Mulliken population analysis, and Born effective charges. The general feature of complex hydrides is the presence of dominant ionic bonding between alkali/alkaline-earth metal and the B, Al or Ga with H complexes. The bonding interaction between H and B, Al or Ga comprises both ionic and covalent character. Generally, the covalent bonding interaction decreases when one goes from B to Al to Ga compounds.

Acknowledgments

The authors gratefully acknowledge the Research Council of Norway for financial support and for the computer time at the Norwegian supercomputer facilities.

References

- [1] <http://www.eere.energy.gov>.
- [2] F.E. Lynch, *J. Less-Common Met.* 172–174 (1991) 943.
- [3] K.H.J. Buschow, H.H. Van Mall, P.D. Googwell, P.S. Rudman, *J. Less-Common Met.* 29 (1972) 203.
- [4] J.H.N. Van Vucht, F.A. Kuijpers, H.C.M. Bruning, *Philips Res. Rep.* 25 (1970) 133.
- [5] K. Yvon, *J. Less-Common Met.* 103 (1991) 53.
- [6] S. Rundqvist, R. Tellgren, Y. Anderson, *J. Less-Common Met.* 101 (1984) 145.
- [7] D.P. Shoemaker, C.B. Shoemaker, *J. Less-Common Met.* 68 (1979) 43.
- [8] C. Switendick, *Z. Phys. Chem. B* 117 (1979) 89.
- [9] B.K. Rao, P. Jena, *Phys. Rev. B* 31 (1985) 6726.
- [10] A. Savin, R. Nesper, S. Wengert, T.F. Fässler, *Angew. Chem. Int. Ed. Engl.* 36 (1997) 1808.
- [11] P. Vajeeston, P. Ravindran, R. Vidya, A. Kjekshus, H. Fjellvåg, *Eur. Phys. Lett.* 72 (2005) 569.
- [12] B. Bogdanovic, M. Schwickardi, *J. Alloys Compd.* 253 (1997) 1.
- [13] G. Kresse, J. Hafner, *Phys. Rev. B* 47 (1993) 558; G. Kresse, J. Furthmüller, *Comput. Mater. Sci.* 6 (1996) 15.
- [14] J.P. Perdew, in: P. Ziesche, H. Eschrig (Eds.), *Electronic Structure of Solids*, Akademie Verlag, Berlin, 1991, p. 11; J.P. Perdew, K. Burke, Y. Wang, *Phys. Rev. B* 54 (1996) 16533; J.P. Perdew, K. Burke, M. Ernzerhof, *Phys. Rev. Lett.* 77 (1996) 3865.
- [15] E. Polak, *Computational Methods in Optimization*, Academic, New York, 1971.
- [16] P. Pulay, *Chem. Phys. Lett.* 73 (1980) 393; D.D. Johnson, *Phys. Rev. B* 38 (1988) 12087.
- [17] H. Hellmann, *Einführung in die Quantumchemie*, Deuticke, Leipzig, 1937; R.P. Feynman, *Phys. Rev.* 56 (1939) 340.
- [18] P.E. Blöchl, *Phys. Rev. B* 50 (1994) 17953; G. Kresse, J. Joubert, *Phys. Rev. B* 59 (1999) 1758.
- [19] P. Vajeeston, P. Ravindran, R. Vidya, H. Fjellvåg, A. Kjekshus, *Phys. Rev. B* 68 (2003) 212101.
- [20] P. Vajeeston, P. Ravindran, R. Vidya, A. Kjekshus, H. Fjellvåg, *Appl. Phys. Lett.* 82 (2003) 2257.
- [21] P. Vajeeston, P. Ravindran, A. Kjekshus, H. Fjellvåg, *Phys. Rev. Lett.* 89 (2002) 175506.
- [22] P. Vajeeston, P. Ravindran, A. Kjekshus, H. Fjellvåg, *Appl. Phys. Lett.* 34 (2004) 84.
- [23] R. Resta, *Rev. Mod. Phys.* 66 (1994) 899.
- [24] <http://www.crystal.unito.it/>.
- [25] J.M. Wills, O. Eriksson, M. Alouani, D.L. Price, in: H. Dreyse (Ed.), *Electronic Structure and Physical Properties of Solids*, Springer, Berlin, 2000.
- [26] V.A. Yartys, R.V. Denys, B.C. Hauback, H. Fjellvåg, I.I. Bulyk, A.B. Riabov, Y.M. Kalychak, *J. Alloys Compd.* 330–332 (2002) 132.
- [27] P. Ravindran, P. Vajeeston, R. Vidya, A. Kjekshus, H. Fjellvåg, *Phys. Rev. Lett.* 89 (2002) 106403.
- [28] P. Vajeeston, P. Ravindran, H. Fjellvåg, A. Kjekshus, *Phys. Rev. B* 70 (2004) 014107.
- [29] M. Kohout, A. Savin, *J. Comput. Chem.* (1997) 181431.
- [30] P. Villars, L.D. Calvert, *Pearson's Handbook of Crystallographic Data for Intermetallic Phases*, vol. 3, American Society for Metals, Materials Park, OH, 1985.
- [31] B.C. Hauback, H.W. Brinks, H. Fjellvåg, *J. Alloys Compd.* 346 (2002) 184.
- [32] B.C. Hauback, H.W. Brinks, C.M. Jensen, K. Murphy, A.J. Maeland, *J. Alloys Compd.* 358 (2004) 142.
- [33] J.P. Bastide, P. Claudy, J.-M. Letoffe, J.E. Hajri, *Rev. Chim. Miner.* 24 (1987) 248.
- [34] B.C. Hauback, H.W. Brinks, R.H. Heyn, R. Blom, H. Fjellvåg, *J. Alloys Compd.* 394 (2005) 35.
- [35] G. Krier, O. Jepsen, A. Burkhardt, O.K. Andersen, *Tight Binding LMTO-ASA Program Version 4.7*, Stuttgart, Germany, 2000; R. Dronskowski, P.E. Blöchl, *J. Phys. Chem.* 97 (1993) 8617.
- [36] P. Vajeeston, P. Ravindran, H. Fjellvåg, A. Kjekshus, *J. Alloys Compd.* 387 (2005) 97.
- [37] P. Vajeeston, P. Ravindran, R. Vidya, H. Fjellvåg, A. Kjekshus, *Cryst. Growth Des.* 4 (2004) 471.
- [38] R.S. Mulliken, *J. Chem. Phys.* 23 (1955) 1833.
- [39] R.D. King-Smith, D. Vanderbilt, *Phys. Rev. B* 47 (1993) 1651; D. Vanderbilt, R.D. King-Smith, *Phys. Rev. B* 48 (1993) 4442.
- [40] H. Morioka, K. Kakizaki, S.C. Chung, A. Yamada, *J. Alloys Compd.* 353 (2003) 310.
- [41] K. Yvon, in: R.B. King (Ed.), *Encyclopedia of Inorganic Chemistry*, vol. 3, Wiley, New York, 1994, p. 1401.
- [42] P. Vajeeston, R. Vidya, P. Ravindran, H. Fjellvåg, A. Kjekshus, A. Skjeltorp, *Phys. Rev. B* 65 (2002) 075101.
- [43] P. Vajeeston, P. Ravindran, A. Kjekshus, H. Fjellvåg, *J. Alloys Compd.* 363 (2003) L7.

- [44] P. Vajeeston, P. Ravindran, A. Kjekshus, H. Fjellvåg, *Phys. Rev. B* 71 (2005) 092103.
- [45] A.F. Wells, *Structural Inorganic Chemistry*, Clarendon, Oxford, 1987.
- [46] J.E. Lowther, J.K. Dewhurst, J.M. Leger, J. Haines, *Phys. Rev. B* 60 (1999) 14485.
- [47] J.P. Bastide, J.C. Bureau, J.M. Létoffé, P. Claudy, *Mater. Res. Bull.* 22 (1987) 185.
- [48] P. Vinet, J. Ferrante, J.R. Smith, J.H. Rose, *J. Phys. C* 19 (1986) L467.
- [49] P. Ravindran, P. Vajeeston, A. Kjekshus, H. Fjellvåg, *Comput. Mater. Sci.* 30 (2004) 349.